International Journal of
Metallurgical & Materials Engineering
Research Article Open Access

Effect of Tin on the corrosion of Mg-5Al based alloy in 3.5 wt.% NaCl Solution

Nguyen Dang Nam[1], Vu Thi Hanh Thu[2] and Nguyen Thi Thanh To[3*]

[1]*Petroleum Department, PetroVietnam University, Ba Ria City, Ba Ria - Vung Tau Province 74000, Vietnam*
[2]*Faculty of Physics and Engineering Physics, University of Science, 227 Nguyen Van Cu Str, Dist 5, Ho Chi Minh City, Vietnam*
[3]*Faculty of Applied Sciences, Ton Duc Thang University, Nguyen Huu Tho Str., Tan Phong Ward, Dist. 7, Ho Chi Minh City, Vietnam*

Abstract

The corrosion resistance of a Mg-5Al alloy was improved by the addition of tin up to 3.0 wt.% due to grain refinement, formation of a protective corrosion product layer, and the lower hydrogen evolution rate. On the other hand, the addition of 4.0 wt.% tin has a deleterious effect on the corrosion resistance of the Mg-5Al alloy in 3.5 wt.% NaCl solution as a result of the higher hydrogen evolution rate that hinder the formation of the protective corrosion product layer.

Publication History:
Received: May 02, 2015
Accepted: December 05, 2015
Published: December 08, 2015

Keywords:

Magnesium alloys, Corrosion test, Electrochemical properties, Microstructure

Introduction

The development of the structural materials in the automotive, electronic and aerospace applications promotes the use of magnesium and its alloys [1]due to many benefit such as high specific strength and energy absorption and low density [2]. Unfortunately, there are still many important questions to be considered for their wider applications in both fundamental and technology. The current focuses of magnesium alloy technology were suggested by Agnewa and Nie [3]. They reported the trends which is a perspective for future research to innovate the alloy properties and extend magnesium alloys' applications. But, the major concern of magnesium and its alloy is poor corrosion resistance [4]. For this reason, the improved corrosion resistance for magnesium alloys has become an important issue to be dealt in the corrosion research field and must be improved to achieve the better corrosion resistance required for their applications. The heavy metals including iron, nickel and copper… were considered as alloying element for magnesium alloys. However, they are highly deleterious because of low hydrogen overvoltage. The aluminum-iron or nickel-magnesium compounds which are formed by iron or nickel impurities, act as local cathodes to form microgalvanic corrosion [5,6]. This requires more active elements to be used as alloying element with reduction potentials closed that of Mg including Al [7,8], Ca [9-11], Sr [12-15] and refines the microstructure by the rapid solidification process [16-19] improved the corrosion resistance. The beneficial effects which they passes to increase in the corrosion resistance of magnesium alloys can be attributed to: (i) decrease in the impurities, (ii) prevention of micro-galvanic couples, (iii) formation of perfect precipitation around finer α-Mg grains, and (iv) ameliorate the surface film [20].

The aluminum addition seems to be the most commonly used due to good castability and corrosion resistance as well as good mechanical properties [20]. Furthermore, $Mg_{17}Al_{12}$ is better corrosion-resistant than α-Mg matrix because it can act as a corrosion barrier [21]. However, when magnesium alloyed with aluminum, it becomes electrochemically more active [23] due to nonuniform Al distribution. Thus, larger amount of aluminum content is referred to an improved corrosion resistance of Mg alloy. Therefore, the effect of a small amount of aluminum (not exceed 5 wt.%) in the Mg alloy is still questionable in case of corrosion resistance. The previous studies [23-29] suggest that the corrosion properties of magnesium alloys depend on the amount of intermetallic phases and inclusions as well as their distribution in the alloy. They act as a corrosion barrier once the less noble α phase was dissolved. β($Mg_{17}Al_{12}$) phase have a passive behavior within a wide pH range resulting in an improved corrosion resistance. However, it also has deleterious influence on corrosion resistance due to microgalvanic corrosion effect [30-31]. Theoretically, impurity elements form microgalvanic corrosion attributed to an effective cathode material in the galvanically couple, or if the nature of the environment inhibits formation or maintenance of a protective film [33,34]. That is the reason why magnesium alloys is poor quality. In addition, the electrical contact between the magnesium alloys and other metals can be insulated or blocked, resulting in reduction in microgalvanic corrosion.

Tin is believed to be an innocuous background material with many applications in the metallurgy industry due to its corrosion resistance. House and Kelsall [35] reported that tin reacts to produce hydrogen in both strongly acidic and alkaline solutions, even though the stability of the valence +2 state is considerably higher. The oxidation of Sn (II) to Sn (IV) proceeds easily in aqueous solutions due to the dissolved oxygen, making Sn (IV) stable in aqueous solutions [36]. An outer SnO_2 layer could be formed on alloy surface for corrosion protection. In addition, Song [37] has reported that the role of tin is to improve the corrosion resistance of magnesium alloys immersed in a corrosive medium. A beneficial effect on corrosion behavior of magnesium alloys can be attributed to the presence of Sn-containing particles and the solute Sn in the matrix phase. It can change the electrochemical anodic and cathodic polarization behavior of the alloy. Therefore, Sn has been strongly considered as an alloying element to improve the corrosion behavior of magnesium alloys. Herein, the study examined the alloying effect of tin on the corrosion behaviour of Mg-5Al based alloy. In order to determine the corrosion behavior of Mg-Al alloys in corroded solutions, Mg-5Al-xSn (x = 0 ÷ 4), alloys are studied based on the basics of electrochemical measurements. The surface products were analyzed by X-ray photoelectron spectroscopy (XPS).

***Corresponding Author:** Nguyen Thi Thanh To, Faculty of Applied Sciences, Ton Duc Thang University, Nguyen Huu Tho Str., Tan Phong Ward, Dist. 7, Ho Chi Minh City, Vietnam, Tel. +84 984 219 234; E-mail: nttto.c3tcvan@khanhhoa.edu.vn

Citation: Nam ND, Thu VTH, To NTT (2015) Effect of Tin on the corrosion of Mg-5Al based alloy in 3.5 wt.% NaCl Solution. Int J Metall Mater Eng 1: 118. doi: http://dx.doi.org/10.15344/2455-2372/2015/118

Citation: Nam ND, Thu VTH, To NTT (2015) Effect of Tin on the corrosion of Mg-5Al based alloy in 3.5 wt.% NaCl Solution. Int J Metall Mater Eng 1: 118. doi: http://dx.doi.org/10.15344/2455-2372/2015/118

Experimental Procedure

Specimen preparation

Pure Mg (99.9 %) ingot was melted in a stainless steel crucible under the protection of gas mixture containing SF_6 and CO_2. The calculated amounts of 5 wt.% of Al: 1, 2, 3, and 4 wt.% Sn were added to Mg melt. After solidification, the ingots were subjected to homogenizing treatment at 400°C for 14 h. The homogenized ingots were machined, which were used as raw materials for extrusion. The extrusion of billets was performed at 320°C. Table 1 summarizes the alloy designation and the corresponding chemical composition of each alloy. The chemical compositions of tested alloys were determined by means of elaboration method. Alloys with chemical compositions used, were 0.010 Mn, 0.005 Si, 0.004 Fe, 0.003 Cu, 0.007 Ni, while the difference between measured and specified composition of tin and aluminum is imperceptible. The specimens for electrochemical tests were first cold-mounted on a mounting cup and then finished by grinding with 600-grit silicon carbide (SiC) paper.

Samples	Composition (wt.%)
# 1	5 Al, bal Mg
# 2	5 Al, 1 Sn, bal Mg
# 3	5 Al, 2 Sn, bal Mg
# 4	5 Al, 3 Sn, bal Mg
# 5	5 Al, 4 Sn, bal Mg

Table 1: Nominal composition of the alloys examined.

Electrochemical investigation methods

All of the electrochemical experiments were performed at room temperature in 3.5 wt.% NaCl solution. The exposed area was 1 cm^2. Potentiodynamic polarization tests were performed using an EG&G PAR 263A potentiostat for the DC measurements. A graphite counter electrode was used, with a saturated calomel electrode as the reference electrode. Prior to the potentiodynamic polarization test, the samples were kept in the solution for 1 h in order to stabilize the open-circuit potential. The potential of the electrodes was swept at a rate of 0.166 mV/s in the range from the initial potential of -250 mV versus E_{corr} to the final potential of -1.3V_{SCE}. The electrochemical impedance spectroscopy (EIS) and corrosion potential measurements were conducted using a IM6e system with a commercial software program for AC measurements. The amplitude of the sinusoidal perturbation was 10 mV. The frequency range was from 100 kHz to 10 mHz. The hydrogen evolution rate of the alloys was investigated by immersion tests. The specimens, with dimensions of 10 mm × 10 mm × 2 mm, were prepared by grinding each side with 600-grit silicon carbide (SiC) paper and degreasing the surfaces with ethanol prior to corrosion testing. The hydrogen evolution rate was used as an indicator of the corrosion rate which was monitored after 1 hour.

Surface analyses

The crystal structure of the Mg-5Al-xSn specimens was investigated by XRD using Cu Kα radiation. For the observation of the microstructure using optical microscope, the specimens were mechanically sanded with sand paper (#220, 600, 1200, 2000, and 4000) and then with 0.1 μm alumina powders. These specimens were then etched in a mixture of acetic acid (10 ml), picric acid (5 g), distilled water (10 ml) and ethanol (70 ml of 95% purity). To investigate the relationship between the electrochemical behavior and surface morphology, the specimens were examined by scanning electron microscopy (SEM) after 6 h of immersion test. The surface products were examined by X-ray photoelectron spectroscopy (XPS) after 1 h of the open-circuit potential.

Results and Discussion

Alloy microstructure

Microstructures of Mg-5Al-xSn alloys with different Sn-containing alloys are shown in Figure 1. It showed the typical microstructure of an alloy and there were no second phases such as $Mg_{17}Al_{12}$ and Mg-Zn compounds located at the grain boundary. It could be attributed to the dissolution of those compounds into the α-Mg matrix. It can be noted that the grain size distributions were homogeneous due to the homogenizing treatment at 400°C prior to 14 h. It also can be seen that a large amount of new fine grains appeared at the grain boundary in the Sn-containing specimens due to recrystallization. The grain size decreased with an increasing of Sn addition.

Figure 2 shows the XRD pattern of Mg-5Al-xSn alloys. All specimens have the defined peaks of Mg and $Mg_{12}Al_{17}$ reflections, new peaks are also detected in the case of Sn-containing specimens. The new peaks are close to the reflections of Mg_2Sn. Importantly, the peak positions of Mg_2Sn coincides well with those of standard XRD patterns, suggesting that the main second phase in the homogenized condition is Mg_2Sn. It was also noted that the intensities of the Mg_2Sn phases increase with increasing of Sn content, implying that the solubility of Sn in Mg varies with the Sn content in Mg-5Al alloy. In addition, no $Mg_{12}Al_{17}$ and Mg_2Sn particles are present at the grain boundaries, indicating that they were completely dissolved into the α-Mg matrix during the heat-treatment.

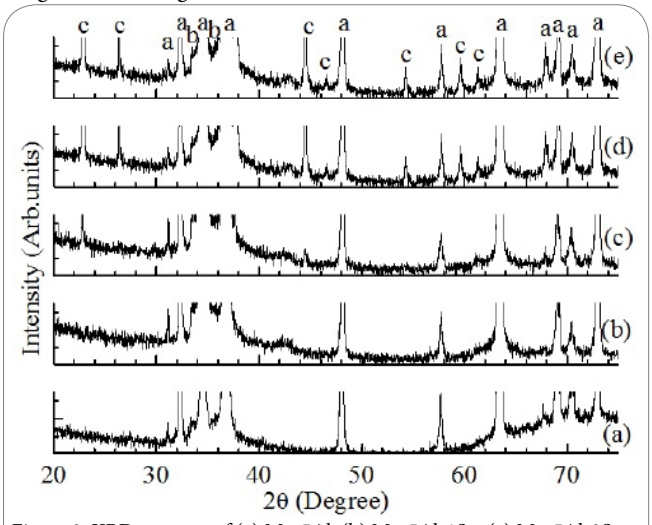

Figure 2: XRD patterns of (a) Mg-5Al, (b) Mg-5Al-1Sn, (c) Mg-5Al-2Sn, (d) Mg-5Al-3Sn, and (e) Mg-5Al-4Sn alloys: a; α-Mg, b; $Mg_{17}Al_{12}$, and c; Mg_2Sn.

Electrochemical properties

Figure 3 shows the polarization curves of the Mg-5Al alloys as a function of the Sn content in 3.5 wt.% NaCl solution. The results showed that all specimens exhibited only active behavior where the anodic current increased with increasing potential, indicating the absence of a passive film on the specimen surface. The potentiodynamic polarization tests indicated that the addition of Sn from 0 to 3 wt.% decreased the corrosion current density. Further additions of Sn from 3 to 4 wt.% Sn increased the corrosion current density considerably. Table 2 lists the corrosion properties.

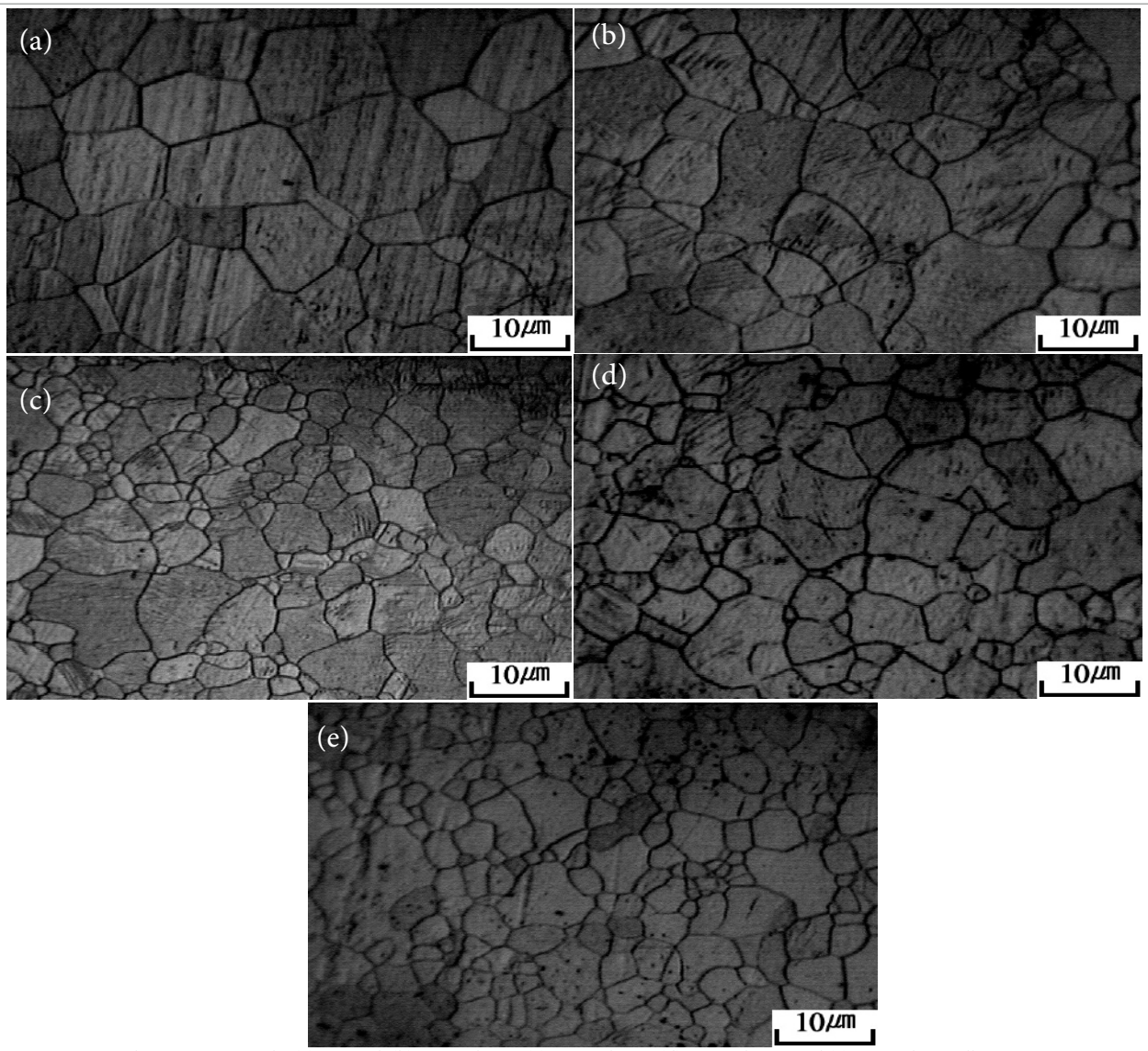

Figure 1: Optical microscope results (a) Mg-5Al, (b) Mg-5Al-1Sn, (c) Mg-5Al-2Sn, (d) Mg-5Al-3Sn, and (e) Mg-5Al-4Sn alloys.

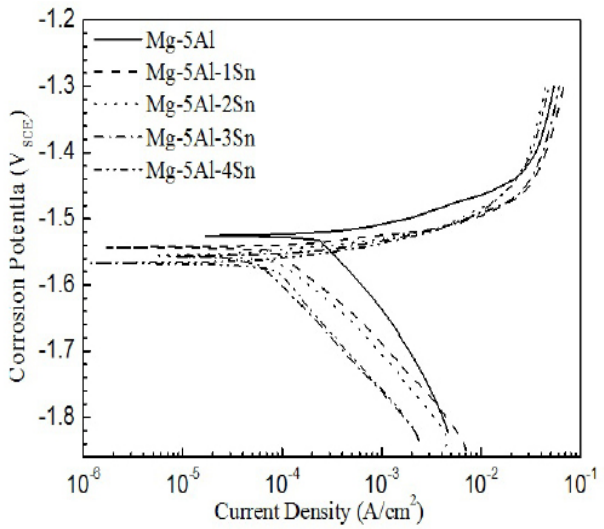

Figure 3: Potentiodynamic polarization curves of Mg-5Al as a function of Sn content.

Figures 4a and Figure 4b present the Nyquist and Bode plots after immersion for 1 h at E_{corr}. The high spectra are used to detect the local surface defects, whereas the medium and low frequency spectra detect the processes within the corrosion product and at the metal/corrosion product interface, respectively. The impedance spectrum of the Mg-5Al-xSn alloy exhibits a capacitive loop in the high frequency range and an inductive loop in the low frequency range. The aperture of impedances and impedance modulus |Z| of the Sn-containing alloys are greater than that of the Mg-5Al alloy. The measured spectra were fitted by the ZSimpWin program with a defined equivalent circuit in Figure 5 a. Where, R_s is the solution resistance, CPE_{dl} is double layer capacitance and R_{ct} is the charge transfer resistance of the magnesium alloys, L and R_L are the inductance and resistance which represented the breakdown of partial protective film on alloy surface [38]. In this case, the capacitor was replaced with a CPE to improve the fitting quality, where the CPE includes a double-layer capacitance (C) and phenomenological coefficient (n). The CPE is a useful modeling element with impedance given by the following equation [39]:

$$\frac{1}{Z} = Q_0 (j\omega)^n \quad (1)$$

Sample	E_{corr} (V_{SCE})	i_{corr} (μA/cm²)	β_a (V/decade)	$-\beta_c$ (V/decade)
#1	-1.534	367.04	0.048	0.197
	-1.546	370.90	0.025	0.172
	-1.540	366.22	0.023	0.161
Average	-1.540	329.17		
#2	-1.547	96.78	0.018	0.144
	-1.571	99.46	0.030	0.172
	-1.566	99.23	0.029	0.169
Average	-1.561	98.49		
#3	-1.544	96.21	0.033	0.188
	-1.553	95.97	0.031	0.169
	-1.548	95.17	0.030	0.152
Average	-1.548	95.78		
#4	-1.563	68.99	0.018	0.141
	-1.565	74.68	0.019	0.171
	-1.563	70.69	0.018	0.165
Average	-1.564	71.45		
#5	-1.568	102.30	0.021	0.138
	-1.557	137.40	0.020	0.139
	-1.561	122.34	0.022	0.141
Average	-1.562	120.68		

Table 2: Critical parameters from potentiodynamic polarization curves for Mg-5Al-xSn alloys in 3.5 wt.% NaCl as a function of Sn addition.

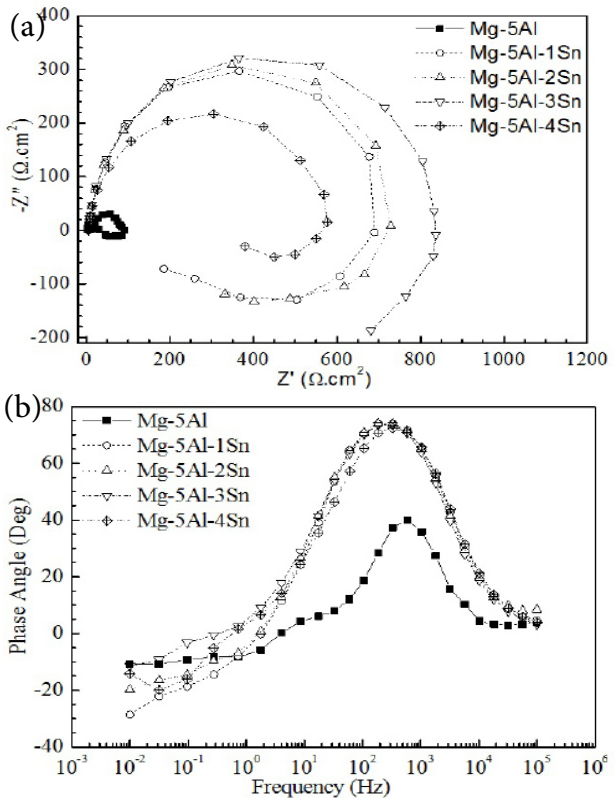

Figure 4: Impedance spectra on (a) Nyquist plots and (b) Bode plots.

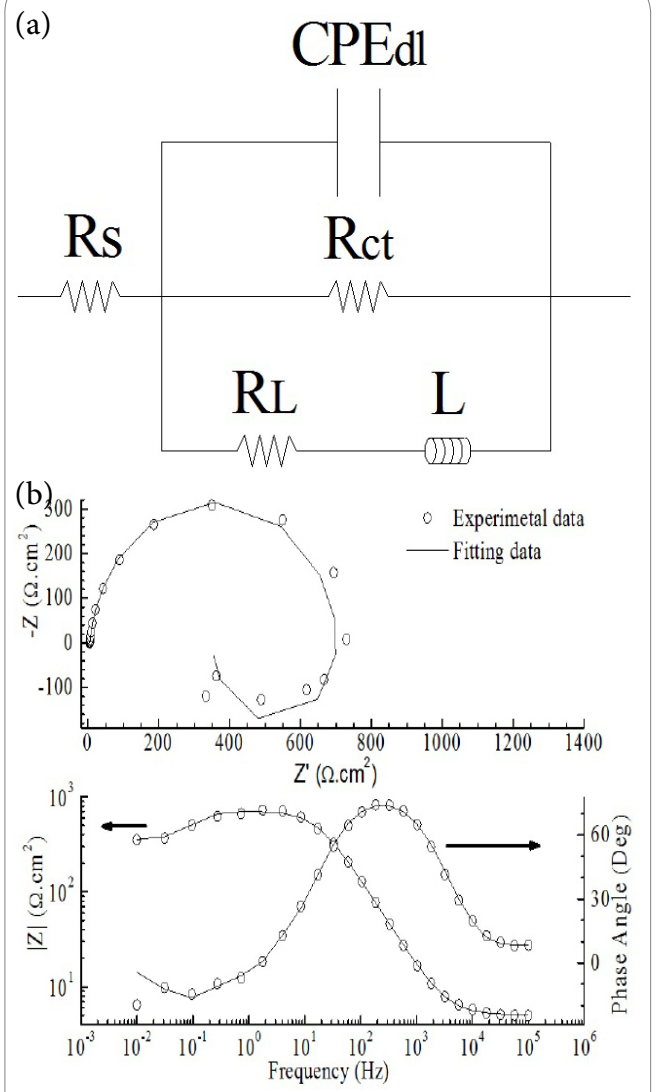

Figure 5: (a) equivalent circuit for fitting the EIS data and (b) fitting results of EIS spectra using an indicated circuit model.

where Q_0 is the admittance that is equal to the inverse of the impedance (Z) at ω = 1 rad/s, j is an imaginary number and n is the CPE power. The n value of a CPE indicates its meaning: n = 1, capacitance; n = 0.5, Warburg impedance; n = 0, resistance and n = -1, inductance. The polarization resistance, R_p, can be calculated from the equivalent circuit as shown below:

$$R_p = R_s + \frac{R_L \times R_{ct}}{R_L + R_{ct}} \quad (2)$$

Figure 5b shows fitting results for experimental impedance spectra of the Mg-5Al-xSn alloys in 3.5 wt.% NaCl solution. The quality of the fitting to the equivalent circuit is judged on the basis of the % error and Chi-square (χ^2) value. Fitting results showed that the % error and χ^2 value were in agreement, suggesting the development of processes are suitable for the defined equivalent circuit. The fitting results are presented in Table 2. It indicates that resistances of Sn-containing specimens are much higher than that of Mg-5Al based alloy.

Hydrogen evolution rate of the Mg-5Al-xSn alloys immersed in 3.5 wt.% NaCl is shown in Figure 6 a. It showed that in a 7 h immersion, hydrogen evolution rate of the Mg-5Al-xSn decreased in the order:

Mg-5Al > Mg-5Al-4Sn > Mg-5Al-1Sn > Mg-5Al-2Sn > Mg-5Al-3Sn. This means that the Mg-5Al-3Sn alloy exhibited the best corrosion resistance, and the Mg-5Al had the lowest corrosion resistance. Corrosion rate of the Mg-5Al-xSn alloys were calculated based on the emitted hydrogen volume and presented in Figure 6b. It indicated that the corrosion rate of the Sn-containing samples increased slightly during 7 h, while it increased quickly in case of Mg-5Al based alloy. The lower corrosion rate could be attributed to the formation of a protective corrosion product layer.

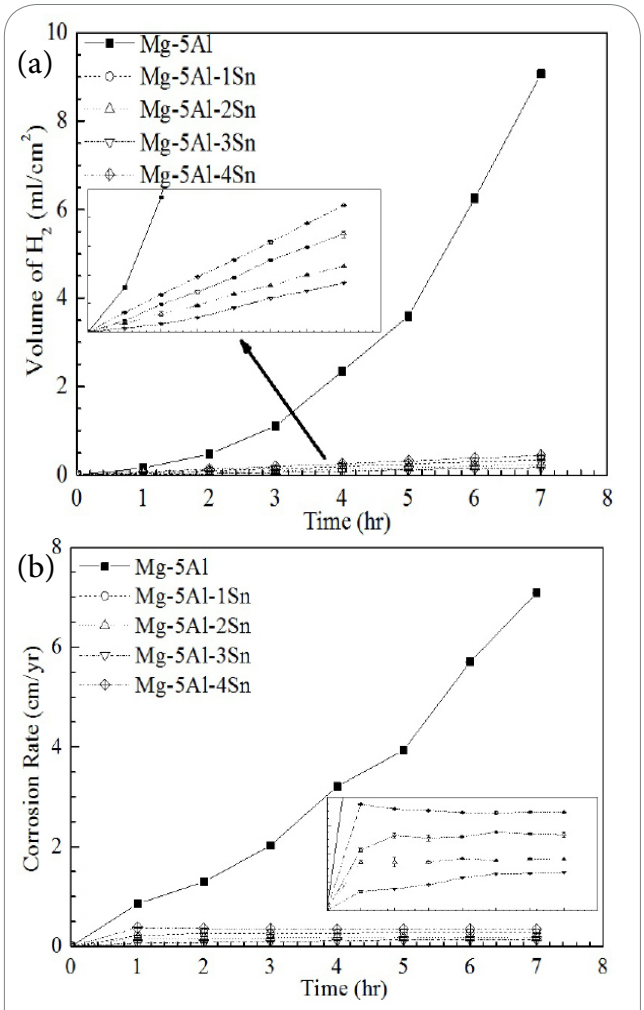

Figure 6: (a) hydrogen evolution and (b) corrosion rate curves of the Mg-5Al-xSn samples immersed in 3.5 wt.% NaCl at room temperature.

Figure 7 shows the change in corrosion rates of the Mg-5Al-xSn alloys. This suggests that the addition of Sn improves the corrosion properties of Mg-5Al based alloy. Average corrosion rate for Mg-5Al-xSn alloys obtained by hydrogen evolution and electrochemical methods are compared in Figure 7. The corrosion rate can be confirmed by the corrosion current density according to Faraday's law and hydrogen evolution rate. The corrosion rate of Mg-5Al-xSn alloys in the electrochemical tests was calculated by Faraday's law [40,41]:

$$\text{Corrosion rate (cm/y)} = \frac{3.16\times10^{7}\times i_{corr}\times M}{z\times F\times\rho} \quad (3)$$

where 3.16 x 10^7 is the metric and time conversion factor, icorr is the corrosion current density (A/cm^2), M is the molar mass of the metal (g/mol), z is number of electron transferred per metal atom, F is the Faraday's constant, and ρ is the density of the metal (g/cm3). Polarization resistance (Rp) value was obtained from EIS data according to eq. (4) [41]:

$$R_p = \frac{\beta_\alpha\times\beta_c}{2.3\times i_{corr}(\beta_\alpha+\beta_c)} \quad (4)$$

where β_a and β_c are the anodic and cathodic Tafel slope, respectively. The corrosion current density of the alloys was calculated using Equation 4 under the assumption that β_a and β_c were equal 0.1 V/decade. Similarly, corrosion rate of the alloys was calculated from the the EIS measurements by using Equation 3 [42-44]. In addition, the hydrogen evolution volume rate, V_H (ml/cm^2.d) can be related to the corrosion rate as, P_H (cm/y) = 0.2279 V_H [45-47]. The results suggested that Sn-containing alloys have lower corrosion rates than Mg-5Al based alloy. Hence, the electrochemical and hydrogen evolution measurements indicate that the corrosion behaviour of Mg-5Al alloy was improved by Sn addition. This improvement could be related to the formation of a protective film on the alloys.

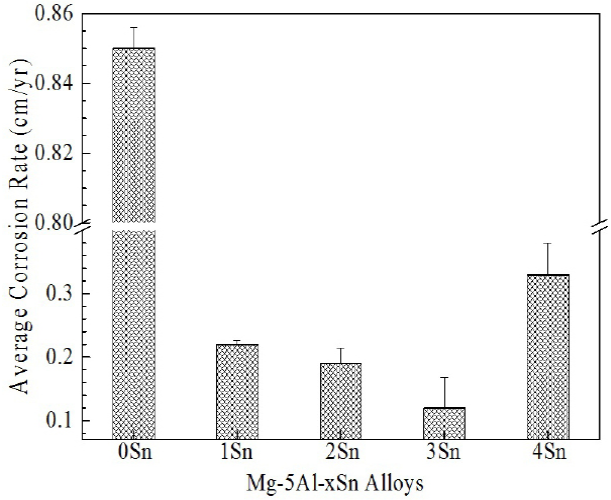

Figure 7: Comparison of the corrosion rates among potentiodynamic polarization, EIS, and the hydrogen evolution measurements in 3.5 wt.% NaCl at room temperature.

Surface analyses

Figure 8 shows SEM images of the surface morphology after 7 hours immersion. There was a significant difference in the surface morphology of the alloys, due to the pitting, which was inwardly penetrated of Cl^- ion. No pitting was observed on the surface of the Mg-5Al-3Sn alloy, whereas there was pitting corrosion on the Mg-5Al, Mg-5Al-1Sn, Mg-5Al-2Sn, and Mg-5Al-4Sn specimens.

X-ray photoelectron spectroscopy was performed to characterize the changes after exposing the alloys to the 3.5 wt.% NaCl solution for 1 h at room temperature. Figure 9 shows the XPS full range survey spectra of the samples, which clearly showed peaks for Mg 2s, Al 2p, Sn 3d, Cl 2p, and O 1s, indicating the existence of Mg, Al, Sn, Cl, and O on the specimen surface. Oxygen KLL [48,49] was also detected on the surface. Figure 9 (b-f) shows the XPS spectra of Mg 2s, Al 2p, Sn 3d, Cl 2p, and O 1s on the alloy surfaces. Mg 2s was observed on the surface of the Sn-containing alloys, whereas there was no Mg 2s present on the Mg-5Al based alloy. The Mg 2p and Al 2p spectra correspond to $MgO/Mg(OH)_2$ and $Al_2O_3/Al(OH)_3$ on the surface of the alloys. This figure also shows that the concentration of Al 2p and O 1s increased with increasing Sn content of 3 wt.% Sn, and decreased with further increase in Sn content. The binding energy of Sn 3d3/2 and Sn 3d5/2 was approximately 494 and 485 eV, respectively Figure 9d. The presence of SnO_2 on the surface of the Sn-containing alloys

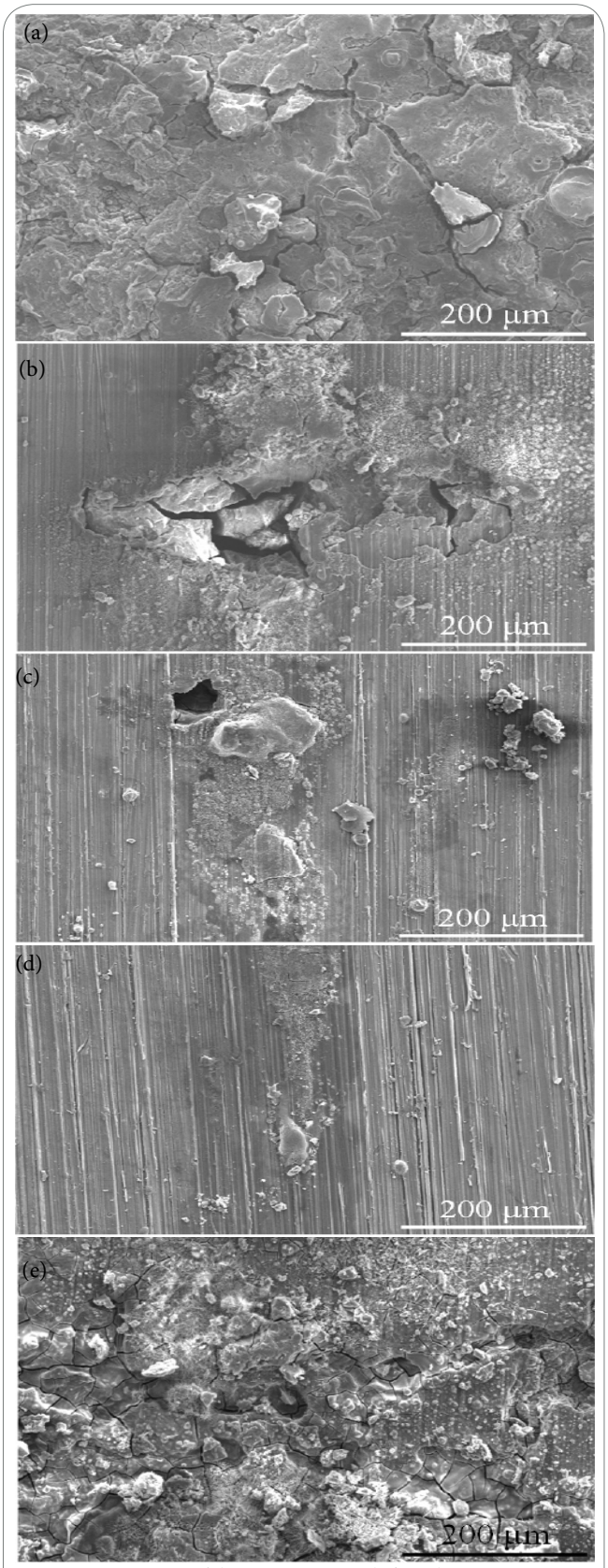

Figure 8: SEM images of the specimens tested after 6 h immersion in 3.5 wt.% NaCl at room temperature: (a) Mg-5Al, (b) Mg-5Al-1Sn, (c) Mg-5Al-2Sn, (d) Mg-5Al-3Sn, and (e) Mg-5Al-4Sn alloys.

decreased the corrosion rate due to a decrease in the hydrogen evolution rate. Compared to the Sn 3d oxide peaks in Figure 8d, the alloy contribution for the 3 wt.% Sn-containing alloy has higher peaks than those peaks from other alloys. In addition, the O 1s spectra were composed of three peaks corresponding to the signals from oxygen in the oxide at 530.05 eV and oxygen in the hydroxyl groups at 531.70 eV. In addition, a lower Cl peak was observed in the Mg-5Al-3Sn specimen. This suggests that the enriched Mg, Al, and Sn products containing played an important role in improving the corrosion products of magnesium alloys, which impeded the adsorption of Cl^- ions.

Discussion

Five different tin-containing Mg-5Al alloys, 0, 1, 2, 3, and 4 wt.% additions, were studied. The microstructural study including OM and XRD suggests that a decrease in grain size of the α-Mg solid solution phase was the major change in the microstructure caused by the addition of Sn. The electrochemical study suggests that the addition of 3 wt.% Sn results in the lowest corrosion rate and hydrogen evolution rate in a corrosive environment. The corrosion resistance mechanism of the alloys can be related to the finer α-Mg grains and no $Mg_{12}Al_{17}$ and Mg_2Sn particles remaining at the grain boundaries, which strongly affect the corrosion performance through control of the microstructure. Therefore, a higher level of total resistance, lower corrosion rate and hydrogen evolution reaction rate were obtained with increasing Sn addition to Mg-5Al alloy in the range, 0 to 3 wt.%, as shown in Table 3 and Figures 4, 6, and 7. Corrosion of Mg can convert metallic Mg to the stable ion Mg^{++}. The overall corrosion reaction is:

$$Mg + 2H_2O \rightarrow Mg(OH)_2 + H_2 \quad (5)$$

The reaction (5) is expressed as the sum of the following reactions:

$$Mg \rightarrow Mg^{2+} + 2e^- \quad (6)$$

$$2H_2O + 2e^- \rightarrow 2OH^- + H^2 \quad (7)$$

$$Mg^{2+} + 2OH^- \rightarrow Mg(OH)^2 \quad (8)$$

Furthermore, magnesium oxide (MgO) was observed due to the following reduction reactions:

$$Mg^{2+} + H_2O \rightarrow MgO + 2H^+ \quad (9)$$

Specimen	R_s ($\Omega.cm^2$)	CPE_{dl}		R_{ct} ($\Omega.cm^2$)	L ($H.cm^2$)	R_L ($\Omega.cm^2$)
		C_{dl} (µF/cm^2)	n (0~1)			
# 1	28.0	23.6	0.9074	104.0	68	78
# 2	4.8	18.8	0.9180	670.6	1277	573
# 3	5.1	18.3	0.9190	704.5	1701	628
# 4	6.0	17.9	0.9240	826.5	2136	782
# 5	5.1	20.9	0.9073	658.2	1116	370

Table 3. Electrochemical impedance measurements.

Therefore, magnesium oxides/hydroxides ($MgO/Mg(OH)_2$) should form on the surface of magnesium upon its exposure to the corrosive environment [50]. Based on the Pourbaix diagram of the Sn/H_2O system [35] and the surface characteristics of the Sn-containing alloys in 3.5 wt.% NaCl solution, the formation of SnO_2 in this environment

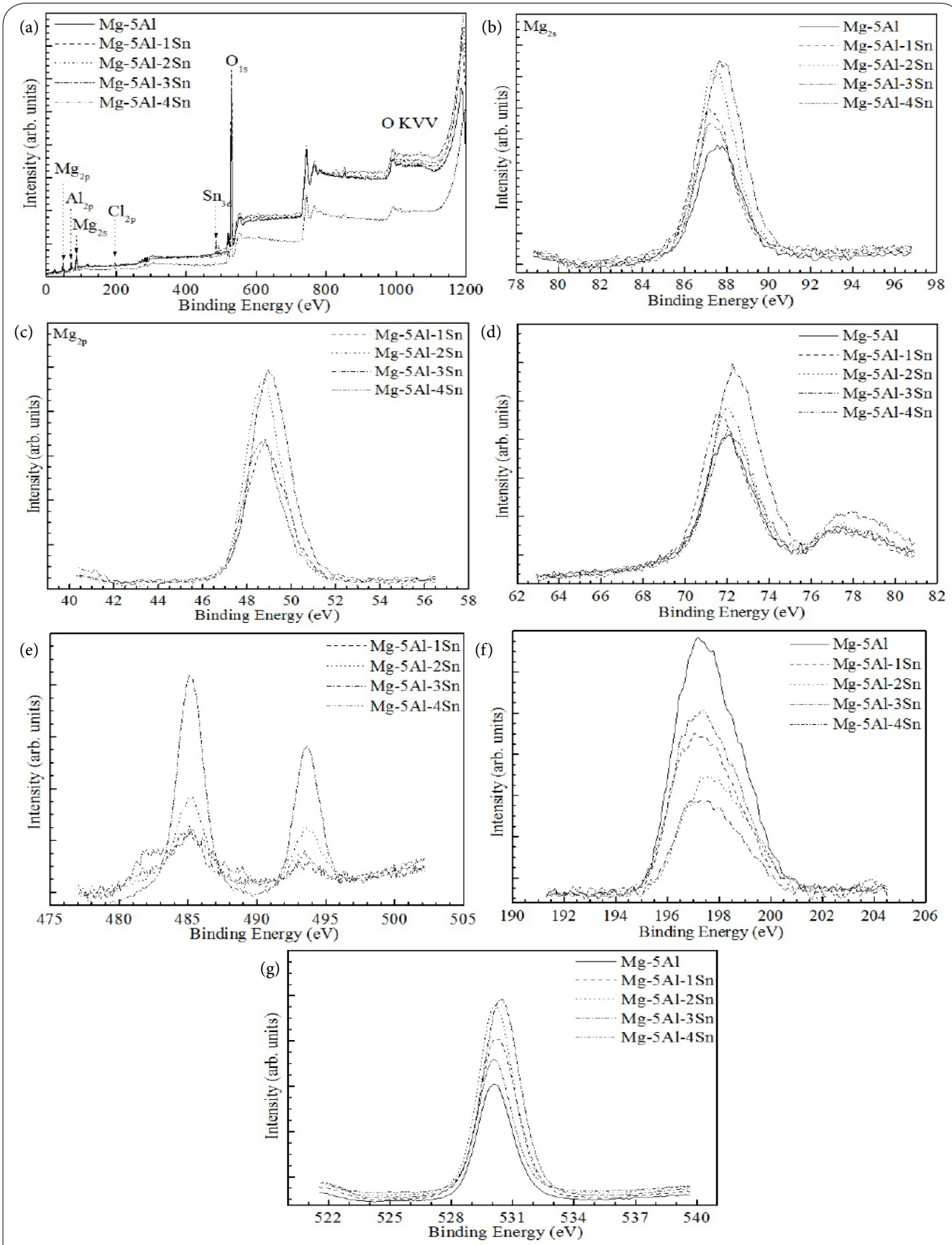

Figure 9: XPS peak analysis for the surface products of the Mg-5Al-xSn alloys: (a) survey scan spectra and narrow scan spectra of (b) Mg, (c) Al, (d) Sn, (e) Cl, and (f) O.

was proposed to proceed through the following reaction scheme:

$$Sn + 4H_2O \rightarrow Sn(OH)_4 + 4e^- + 4H^+ \quad (10)$$

Sn may also be oxidized according to the following reactions:

$$Sn + 2H_2O \rightarrow Sn(OH)_2 + 2e^- + 2H^+ \quad (11)$$
$$Sn(OH)_2 + 2H_2O \rightarrow Sn(OH)_4 + 2e^- + 2H^+$$

The following dehydration reaction can take place [51]:

$$Sn(OH)_4 \rightarrow SnO_2 + 2H_2O$$

Therefore, when Sn was added to the alloy, the Sn oxide was enriched in the indicated content range due to the occurrence of Sn oxides through the formation of a corrosion product layer, as shown in Figure 9d. The surface characteristics revealed SnO_2 to be the main oxide. Therefore, the difference in total resistance and hydrogen evolution rate is caused by a difference in the composition and quantity of surface products formed on the alloy surfaces. However, total resistance increased and hydrogen evolution rate decreased strongly with increasing Sn content from 0 to 3 wt.% Sn due to surface film formation, and decreased with further increases in Sn content. The corrosion products formed is certainly dense enough to protect the alloy surface during the lengthy immersion time. For 0 ÷ 3 wt.% Sn specimens, the protection layer that formed in the initial stage of the alloy surface can prevent the metal from being corroded further. Grain refinement can increase the number of active atoms on the surface, accelerating the formation of the protective layer. Therefore, Sn addition (0 ÷ 3 wt.%) with grain refinement has an increase in the corrosion resistance of Mg-5Al alloy. This results in the formation of an oxide protection layer. This is attributed to the uniform distribution of Sn in the α-Mg matrix, and is also related to the uniform distribution of Sn oxides on the growth of corrosion products. There is a general hindrance of corrosion from the fresh surface of Sn oxides. This might be related to the observation that grain refinement and sufficient second phase have a lower tendency for localized grain boundary corrosion, whereas in higher second phase (Mg_2Sn) containing specimen, this can result in failure when pitting effect arises, as shown in Figure 8e. It can begin as local galvanic attack relating to the Mg_2Sn phase distribution and Mg. In addition, the polarization may reduce the potential difference of the couple as the galvanic current develops. These accelerate the combination of atomic H on surfaces to form the hydrogen gas that evolves. Therefore, the decrease in the corrosion resistance of Mg-5Al-4Sn was performed. This is coincident with the results shown in the electrochemical and surface analyses. In summary, the results suggest that the corrosion behaviour of Mg-5Al alloy can be improved by the addition up to 3 wt.% Sn. On the other hand, the addition of 4 wt.% Sn accelerates the corrosion rate of Mg-5Al alloy. Clearly, the presence of beneficial Sn compounds on the outer layer of the protective film inhibits the ability of chloride ion to penetrate and destroy the alloy. The beneficial Sn compounds might concentrate the protection of the corrosion product layers. In the case of 0 ÷ 3 wt.% Sn alloy, the Sn concentration was sufficient to act as a barrier to Mg-5Al alloy dissolution, which enhances the corrosion properties of alloy. On the other hand, the higher Sn content in the 4 Sn alloy had a higher corrosion rate.

Conclusion

The major changes in the microstructure caused by the addition of Sn were the decrease in grain size of the α-Mg phase and increase of Mg_2Sn phase in the Mg matrix. The corrosion rate decreased with increasing Sn. However, the addition of 4 wt.% Sn did not improve the corrosion resistance due to acceleration of the hydrogen evolution reaction rate. The corrosion products on the surface of the Sn specimens added from 0 to 3 wt.%, which was composed mainly of SnO, could improve the corrosion resistance of the Mg-5Al alloys in 3.5 wt.% NaCl solution.

Competing Interests

The authors have no competing interests with the work presented in this manuscript.

Author Contributions

All the authors substantially contributed to the study conception and design as well as the acquisition and interpretation of the data and drafting the manuscript.

Acknowledgement

The authors are grateful for the support of Vietnam Oil & Gas Group, PetroVietnam University.

References

1. Makar GL, Kruger J (1990) Corrosion studies of rapidly solidified magnesium alloys. J Electrochem Soc 137: 414-421.
2. Schumann S, Friedrich H (2006) Engineering requirements, strategies and examples, in: Magnesium Technology, Metallurgy, Design Data, Applications. H.E. Friedrich, B.L. Mordike (Eds.), Berlin 677.
3. Agnewa SR, Nie JF (2010) Preface to the viewpoint set on: The current state of magnesium alloy science and technology. Scripta Mater 63: 671-673.
4. Hillis JE (1983) The effects of heavy metal contamination on magnesium corrosion performance. Light Met Age 41: 25-29.
5. Abhijeet SB, Balasubramaniam R, Gupta M (2008) Corrosion behaviour of Mg-Cu and Mg-Mo composites in 3.5 % NaCl. Corros Sci 50: 2423-2428.
6. Liu M, Uggowitzer PJ, Nagasekhar AV, Schmutz P, Easton M, et al. (2009) Calculated phase diagrams and the corrosion of die-cast Mg-Al alloys. Corros Sci 51: 602-619.
7. Prasad A, Shi Z, Atrens A (2012) Influence of Al and Y on the ignition and flammability of Mg alloys. Corros Sci 55: 153-163.
8. Khaselev O, Weiss D, Yahalom J (2001) Structure and composition of anodic films formed on binary Mg-Al alloys in KOH-aluminate solutions under continuous sparking. Corros Sci 43: 1295-1307.
9. Nam ND (2014) Corrosion behavior of Mg-5Al based magnesium alloy with 1 wt.% Sn, Mn and Zn additions in 3.5 wt.% NaCl solution. J Magnesium Alloys 2: 190-1995.
10. Kim KH, Nam ND, Kim JG, Shin KS, Jung HC (2011) Effect of calcium addition on the corrosion behavior of Mg-5Al alloy. Intermetallics 19: 1831-1838.
11. Lisitsyn V, Hamu GB, Eliezer D, Shin KS (2009) The role of Ca microalloying on the microstructure and corrosion behavior of Mg-6Zn-Mn-(0.5-2)Si alloys. Corros Sci 51: 776-784.
12. Kim WC, Nam ND, Kim JG, Lee JI (2011) Effect of strontium on corrosion properties of AZ91 magnesium alloy. Electrochem Solid-State Lett 14: C21-C24.
13. Ghali E, Dietzel W, Kainer KU (2004) Testing of general and localized corrosion of magnesium alloys: A critical review. J Mater Eng Perf 13: 517-529.
14. Janz A, Grobner J, Mirkovic D, Medraj M, Zhu J, et al. (2007) Experimental study and thermodynamic calculation of Al-Mg-Sr phase equilibria. Intermetallics 15: 506-519.
15. Nam ND, Kim WC, Kim JG, Shin KS, Jung HC (2011) Corrosion resistance of Mg-5Al-xSr alloys. J Alloys Compd 509: 4839-4847.
16. Bian MZ, Tripathi A, Yu H, Nam ND, Yan LM (2015) Effect of aluminum content on the texture and mechanical behavior of Mg-1 wt.% Mn wrought magnesium alloys. Mater Sci Eng A 639: 320-326.

17. Yamasaki M, Hayashi N, Izumi S, Kawamura Y (2007) Corrosion behavior of rapidly solidified Mg-Zn-rare earth element alloys in NaCl solution. Corros Sci 49: 255-262.

18. Birbilis N, Easton MA, Sudholz AD, Zhu SM, Gibson MA (2009) On the corrosion of binary magnesium-rare earth alloys. Corros Sci 51: 683-689.

19. Nam ND, Mathesh M, Le TV, Nguyen TH (2014) Corrosion behavior of Mg-5Al-xZn alloys in 3.5 wt.% NaCl solution. J Alloys Compd 616: 662-668.

20. Arrabal R, Pardo A, Merino MC, Mohedano M, Casajús P, et al. (2012) Effect of Nd on the corrosion behaviour of AM50 and AZ91D magnesium alloys in 3.5 wt.% NaCl solution. Corros Sci 55: 301-312.

21. Nakaura Y, Watanabe A, Ohori K (2006) Effects of Ca, Sr Additions on Properties of Mg-Al Based Alloys. Mater Tran 47: 1031-1039.

22. Cizek L, Greger M, Pawlica L, Dobrzanski LA, Tanski T (2004) Study of selected properties of magnesium alloy AZ91 after heat treatment and forming. J Mater Process Technol 157-158: 466-471.

23. Song GL, Atrens A (1999) Corrosion mechanisms of magnesium alloys. Adv Eng Mater 1: 11-33.

24. Nam ND, Kim WC, Kim JG, Shin KS, Jung HC (2009) Effect of mischmetal on the corrosion properties of Mg-5Al alloy. Corros sci 51: 2942-2949.

25. Jonsson M, Thierry D, LeBozec N (2006) The influence of microstructure on the corrosion behaviour of AZ91D studied by scanning Kelvin probe force microscopy and scanning Kelvin probe. Corros Sci 48: 1193-1208.

26. Pardo A, Merino MC, Coy AE, Viejo F, Arrabal R, et al. (2008) Influence of microstructure and composition on the corrosion behaviour of Mg/Al alloys in chloride media. Electrochim Acta 53: 7890-7902.

27. Song GL, Atrens A (2003) Understanding magnesium corrosion-a framework for improved alloy performance. Adv Eng Mater 5: 837-858.

28. Esmaily M, Mortazavi N, Svensson JE, Halvarsson M, Blücher DB, et al. (2015) Atmospheric corrosion of Mg alloy AZ91D fabricated by a semi-solid casting technique: The influence of microstructure. J Electrochem Soc 162: C311-C321.

29. Nam ND, Kim JG, Shin KS, Jung HC (2010) The effect of rare earth additions on the electrochemical properties of Mg-5Al-based alloys. Scripta Mater 63: 625-628.

30. Abidin NIZ, Martin D, Atrens A (2011) Corrosion of high purity Mg, AZ91, ZE41 and Mg2Zn0.2Mn in Hank's solution at room temperature. Corros Sci 53: 862-872.

31. Galicia G, Pebere N, Tribollet B, Vivier V (2009) Local and global electrochemical impedances applied to the corrosion behaviour of an AZ91 magnesium alloy. Corros Sci 51: 1789-1794.

32. Chen J, Wang J, Han EH, Ke W (2009) In situ observation of pit initiation of passivated AZ91 magnesium alloy. Corros Sci 51: 477-484.

33. Krawiec H, Stanek S, Vignal V, Lelito J, Suchy JS (2011) The use of microcapillary techniques to study the corrosion resistance of AZ91 magnesium alloy at the microscale. Corros Sci 53: 3108-3111.

34. Südholz AD, Kirkland NT, Buchheit RG, Birbilis N (2011) Electrochemical properties of intermetallic phases and common impurity elements in magnesium alloys. Electrochem Solid-State Lett 14: C5-C7.

35. Makar GL, Kruger J (1993) Corrosion of magnesium. Int Mater Rev 38: 138-153.

36. House CI, Kelsall GH (1984) Potential-pH diagrams for the Sn/H2O Cl system. Electrochim Acta 29: 1459-1464.

37. Bard AJ, Parsons R, Jordan J (1985) Standard potentials in aqueous solution. Marcel Dekker Inc New York 848.

38. Song GL (2009) Effect of tin modification on corrosion of AM70 magnesium alloy. Corros Sci 51: 2063-2070.

39. Zhang T, Shao Y, Meng G, Cui Z, Wang F (2011) Corrosion of hot extrusion AZ91 magnesium alloy: I-relation between the microstructure and corrosion behavior. Corros Sci 53: 1960-1968.

40. Macdonald JA (1987) Impedance spectroscopy. John Wiley & Sons 595.

41. Jonse DA (1996) Principles and prevention of corrosion. Printice-Hall NJ 572.

42. Pound BG, Abdurrahman MH, Glucina MP, Wright GA, Sharp RM (1985) The corrosion of carbon steel and stainless steel in simulated geothermal media. Aust J Chem 38: 1133-1140.

43. Nam ND, Kim JG (2010) Effect of niobium on the corrosion behaviour of low alloy steel in sulfuric acid solution. Corros Sci 52: 3377-3384.

44. Kim KH, Lee SH, Nam ND, Kim JG (2011) Effect of cobalt on the corrosion resistance of low alloy steel in sulfuric acid solution. Corros Sci 53: 3576-3587.

45. Nam ND, Mathesh M, Forsyth M, Jo DS (2012) Effect of manganese additions on the corrosion behavior of an extruded Mg-5Al based alloy. J Alloys Compd 542: 199-206.

46. Zhao MC, Liu M, Song G, Atrens A (2008) Influence of the β-phase morphology on the corrosion of the Mg alloy AZ91. Corros Sci 50: 1939-1953.

47. Shi Z, Atrens A (2011) An innovative specimen configuration for the study of Mg corrosion. Corros Sci 53: 226-246.

48. Abidin NIZ, Atrens AD, Martin D, Atrens A (2011) Corrosion of high purity Mg, Mg2Zn0.2Mn, ZE41 and AZ91 in Hank's solution at 37 °C. Corros Sci 53: 3542-3556.

49. Zhong X, Li Q, Hu J, Lu Y (2008) Characterization and corrosion studies of ceria thin film based on fluorinated AZ91D magnesium alloy. Corros Sci 50: 2304-2309.

50. Nam ND, Bian MZ, Forsyth M, Seter M, Tan M, et al. (2012) Effect of calcium oxide on the corrosion behaviour of AZ91 magnesium alloy. Corros Sci 64: 263-271.

51. Shin KS, Bain MZ, Nam ND (2012) Effects of crystallographic orientation on corrosion behavior of magnesium single crystals. JOM 64: 664-670.

52. Nam ND, Kim MJ, Jang YW, Kim JG (2010) Effect of tin on the corrosion behavior of low-alloy steel in an acid chloride solution. Corros Sci 52: 14-20.